ACS Sustainable Chemistry & Engineering

Research Article

pubs.acs.org/journal/ascecg

NiIr Nanoparticles Immobilized on the Pores of MIL-101 as Highly Efficient Catalyst toward Hydrogen Generation from Hydrous Hydrazine

Pingping Zhao,[†] Nan Cao,[†] Jun Su,[§] Wei Luo,*[,†,‡] and Gongzhen Cheng*[,†]

[†]College of Chemistry and Molecular Sciences, Wuhan University, Wuhan, Hubei 430072, People's Republic of China

[‡]Suzhou Institute of Wuhan University, Suzhou, Jiangsu 215123, People's Republic of China

[§]Wuhan National Laboratory for Optoelectronics, Huazhong University of Science and Technology, Wuhan, Hubei 430074, People's Republic of China

Supporting Information

ABSTRACT: Highly dispersed ultrafine NiIr nanoparticles with different compositions were successfully encapsulated into the cavities of MIL-101 and applied to catalyze the dehydrogenation of hydrazine monohydrate. The catalytic activities relied on the composition of metals, support materials, alkaline, as well as the temperature strongly. Among all the catalysts tested, $Ni_{85}Ir_{15}$@MIL-101 exhibited the highest catalytic performance in the presence of NaOH at 50 °C. Even at 25 °C, the $Ni_{85}Ir_{15}$@MIL-101 exhibited the complete dehydrogenation of hydrazine with a turnover frequency value of 24 h^{-1}.

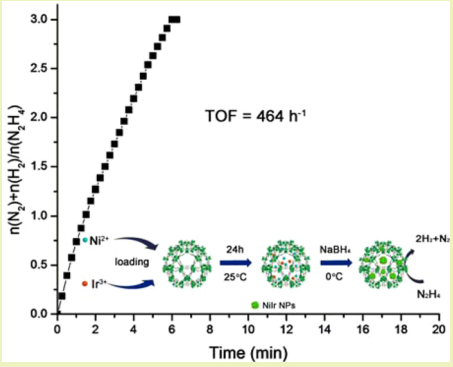

KEYWORDS: *Hydrogen storage, Hydrazine, MIL-101, Ni, Ir*

INTRODUCTION

Hydrogen is a source of clean and environmental-friendly alternative energy addressing typical energy-related issues such as air pollution or global climate change. As a result, numerous efforts have been carried out to construct a "hydrogen economy" society.[1−3] The key constraint to the widespread use of hydrogen energy lies in searching for safe and efficient hydrogen carriers with high hydrogen content, easy handling and transportation, recycling of byproducts, and so on.[4−6] To date, metal hydrides,[7] sorbent materials,[8−10] and chemical hydride systems[11] have been investigated as hydrogen carriers.[12] Among them, liquid-phase hydrogen carriers without the involvement of any solid byproduct, like formic acid (HCOOH),[13−18] liquid organic hydrogen carriers (LOHCs),[19−22] liquid amine borane complexes,[11] and hydrous hydrazine,[23,24] with easy handling and transportation, have been considered more advantageous over traditional solid-phase hydrogen materials.[25−27] Hydrous hydrazine ($N_2H_4·H_2O$), with a hydrogen content of 8.0 wt %, is regarded as a potential hydrogen carrier due to its complete decomposition to hydrogen with only nitrogen as the byproduct via the reaction (eq 1).[28−31] Moreover, nitrogen could be transformed to ammonia and then to hydrazine successively by an electrolytic process to fulfill the easy recharging advantage.[32−34] In view of hydrogen storage application, the undesired pathway decomposed by the reaction (eq 2) must be avoided.[35,36] Thus, a number of unitary and binary metal nanoparticles (NPs) have been developed.[37−41]

$$N_2H_4 \rightarrow N_2 + 2H_2 \quad (1)$$

$$3N_2H_4 \rightarrow 4NH_3 + N_2 \quad (2)$$

Iridium-based catalysts have been widely used for dehydrogenation reaction of hydrazine monohydrate. However, catalyst preparation or hydrazine decomposition only exhibited high selectivity at harsh conditions. For example, Cho et al. reported a set amount of Ir-based catalysts, prepared at high temperatures (>400 °C), and the decomposition of hydrazine were tested at high pressures (i.e., 350 psi).[42,43] Vieira et al. reported the synthesis of Ir/CNF at 680 °C and the decomposition test was carried out at 120 °C under the pressure of 22 or 5.5 bar.[44] Zhang's group reported a two-step synthesis of a NiIr/Al_2O_3 catalyst by reducing the precursor in the H_2 atmosphere at 500 °C to get Ni/Al_2O_3 first, and further reducing in the H_2 atmosphere at 300 °C after being mixed with H_2IrCl_6. This catalyst exhibits a turnover frequency (TOF) value of 6.3 h^{-1} with 99% H_2 selectivity at 30 °C.[45] Recently, the decomposition of liquid-phase hydrazine catalyzed by Ir-based NPs at mild conditions was reported. For example, Xia's group reported

Received: January 6, 2015
Revised: April 27, 2015
Published: April 29, 2015

DOI: 10.1021/acssuschemeng.5b00009
ACS Sustainable Chem. Eng. 2015, 3, 1086−1093

Scheme 1. Scheme of the Synthesis of NiIr@MIL-101 and Its Application to the Hydrogen Generation of $N_2H_4{\cdot}H_2O$

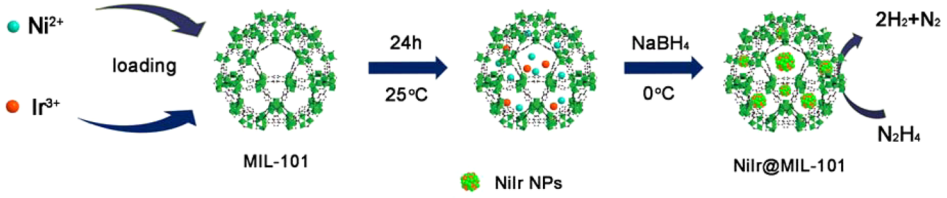

Table 1. Ni−Ir Compositions of the as-Synthesized NiIr@MIL-101 Catalysts Determined by ICP-AES

metal compositions of NiIr@MIL-101	$Ni_{49}Ir_{51}$	$Ni_{71}Ir_{29}$	$Ni_{82}Ir_{18}$	$Ni_{85}Ir_{15}$	$Ni_{90}Ir_{10}$
Ni−Ir of loading	$Ni_{40}Ir_{60}$	$Ni_{60}Ir_{40}$	$Ni_{70}Ir_{30}$	$Ni_{75}Ir_{25}$	$Ni_{80}Ir_{20}$
Ni (wt %)	1.6	2.51	3.45	4.76	5.61
Ir (wt %)	5.4	3.42	2.44	2.73	2.21
Ni+Ir/NiIr@MIL-101 (mmol/100 mg)	0.055	0.077	0.072	0.096	0.107

core−shell octapods and alloyed nanocages PdIr with H_2 selectivity of 66% and 29% respectively at room temperature.[46] Xu's group reported surfactant stabilized NiIr NPs with a TOF value of 1.6 h^{-1} and 100% H_2 selectivity at room temperature.[36] Thus, the development of Ir-based nanocatalysts with 100% hydrogen selectivity and extremely high catalytic activity toward dehydrogenation of hydrazine monohydrate at relatively mild conditions is highly desirable.

On the other hand, metal−organic frameworks (MOFs), possessing large surface area, high porosity, and chemical tunability, have been widely studied in gas storage and separation, sensing, catalysis, and so on.[47−49] The large pore size and relatively small window size of the porous MOFs may facilitate the limitations of shape and diameter of metal NPs in the cavities and further prevent their aggregation.[50−57] Herein, we reported the synthesis of bimetallic NiIr NPs immobilized on MIL-101 and their application in dehydrogenation of hydrazine monohydrate in alkaline solution. MIL-101, a terephthalate-based MOF, was selected as the support for NiIr NPs due to its superiorities of hybrid surface structure, large cavity and diameter, and high thermal and aqueous stability.[58] Among all the catalysts tested, the $Ni_{85}Ir_{15}$@MIL-101 catalyst exhibited a rather satisfactory catalytic activity with 100% hydrogen selectivity toward the decomposition of hydrous monohydrate in alkaline solution, with TOF values of 464 h^{-1} at 50 °C and 24 h^{-1} at 25 °C, respectively.

MATERIALS AND METHODS

Materials. Ammonium fluoride (96 wt %), aqueous hydrofluoric acid (40 wt %), chromic nitrate nonahydrate (99 wt %), nickel chloride hexahydrate (99 wt %), sodium borohydride (96 wt %), terephthalic acid (99 wt %), and ethanol with a purity >99.8 wt % were provided by Sinopharm Chemical Reagent Co., Ltd. Iridium chloride with a purity >99 wt % was purchased from Wuhan Greatwall Chemical Regent Co., Ltd. Hydrazine monohydrate with a purity >98 wt % was provided from TCI Shanghai Co., Ltd. All the chemical regents were used directly.

Synthesis of MIL-101. Porous MOF (MIL-101) was hydrothermally prepared according to the literature.[28] Typically, a mixture of 332 mg of terephthalic acid, 800 mg of $Cr(NO_3)_3{\cdot}9H_2O$, and 0.1 mL aqueous HF in 9.6 mL water was heated at 220 °C for 8 h. The raw products of green powder were further treated in ethanol at 80 °C for 24 h, followed by soaked in a solution of NH_4F with a concentration of 1 M at 70 °C for 24 h to remove the unreacted terephthalic acid. The purified MIL-101 was activated at 150 °C in a vacuum for 12 h.

Synthesis of NiIr@MIL-101. NiIr@MIL-101 catalysts were prepared by a simple impregnation method. In a typical procedure, 100 mg of activated MIL-101 was added to 10 mL of deionized water containing 0.2 mmol metal precursors with varying compositions of $IrCl_3{\cdot}H_2O$ and $NiCl_2{\cdot}6H_2O$ (with Ni/Ir molar ratios of 1:0, 3:2, 2:3, 3:7, 1:3, 1:4, 0:1). After the solution was stirred at room temperature for 24 h, the metal salts were finally loaded into the pores of MIL-101 successfully. And then, 37.8 mg of $NaBH_4$ was added to the solution as a reductant at 0 °C. After centrifugation, the as-synthesized NiIr@MIL-101 catalysts with different Ni/Ir ratios were obtained.

Synthesis of Catalysts with Different supports. The synthesis of catalysts with Different supports (such as γ-Al_2O_3, SiO_2, carbon black) were similar to that of MIL-101.

Hydrazine Monohydrate Decomposition. Typically, a mixture of 100 mg of NiIr@MIL-101 catalyst, 80 mg of NaOH, and 4 mL of water was placed in a 25 mL two-necked flask with stirring at the same time. One neck was slipped with a rubber plug, and the other neck was connected with a gas buret. After 0.1 mL of $N_2H_4{\cdot}H_2O$ was injected into the flask, the decomposition began with gas released. The gas was collected after a filtration treatment of 1 M HCl solution. The value of H_2 selectivity (X) is calculated by eq 3, and the turnover frequency (TOF) is determined by eq 4.

$$X = (3\lambda - 1)/8[\lambda = n(H_2 + N_2)/n(H_2NNH_2)] \quad (n = \text{amount of substance}) \tag{3}$$

$$\text{TOF} = k_{H2}/n_{metal}(k_{H2}\ (\text{mol}{\cdot}\text{h}^{-1}) = \text{hydrogen generation rate}) \tag{4}$$

The decomposition reaction without NaOH was used to test the role of alkaline, with a similar method except that NaOH was not added.

An additional 0.1 mL of $N_2H_4{\cdot}H_2O$ was added into the flask after completion of the previous decomposition to test the reusability of $Ni_{85}Ir_{15}$@MIL-101 catalysts.

To determine the Arrhenius activation energy (E_a), the hydrogen generation of $N_2H_4{\cdot}H_2O$ was carried at the same conditions except that the temperature was controlled at 25, 40, 50, and 60 °C.

Characterization. The characterization of X-ray diffraction (PXRD) profile was measured by a Bruker D8-Advance X-ray diffractometer/PANalytical X'Pert Pro X-ray diffractometer with a velocity of 1° min^{-1} for the low-angle profile and 5° min^{-1} for the wide-angle profile, in which Cu Kα was used as the radiation source with a wavelength of 0.154 178 nm. The N_2 adsorption/desorption pattern was recorded by Quantachrome NOVA 4200e at the temperature of 77 K controlled by the liquid nitrogen. The XPS spectrum was investigated by a Kratos XSAM 800 spectrophotometer. The transmission electron microscopy (TEM) images and the EDX spectrum of the catalysts were obtained from a Tecnai G20 U-Twin transmission electron microscope and the acceleration voltage was kept at 200 kV for the energy-dispersive X-ray (EDX) detector. An Ametek Dycor mass spectrometer was used to test the composition of the gas released (MS profile) under an Ar atmosphere. The inductively

DOI: 10.1021/acssuschemeng.5b00009
ACS Sustainable Chem. Eng. 2015, 3, 1086−1093

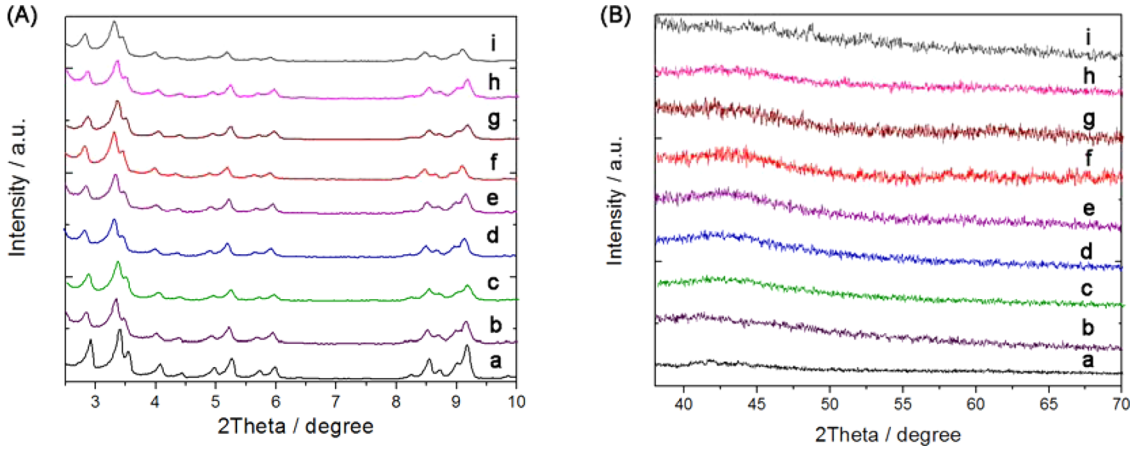

Figure 1. PXRD of low-angle profiles (A) and wide-angle profiles (B): (a) MIL-101; (b) Ir@MI-101; (c) $Ni_{49}Ir_{51}$@MIL-101; (d) $Ni_{71}Ir_{29}$@MIL-101; (e) $Ni_{82}Ir_{18}$@MIL-101; (f) $Ni_{85}Ir_{15}$@MIL-101; (g) $Ni_{85}Ir_{15}$@MIL-101 after five circles of catalytic decomposition of hydrazine monohydrate; (h) $Ni_{90}Ir_{10}$@MIL-101; (i) Ni@MIL-101.

coupled plasma atomic emission spectroscopy (ICP-AES) results were determined by an IRIS Intrepid II XSP (Thermo Fisher Scientific, USA).

RESULTS AND DISCUSSION

The synthesis of NiIr@MIL-101 catalysts are illustrated in Scheme 1. The compositions of Ni and Ir in the NiIr@MIL-101 catalysts are listed in Table 1 according to the ICP-AES results. The low-angle powder X-ray diffraction profiles of all the samples in Figure 1A indicate no obvious collapse of the intrinsic structure of MIL-101 after the immobilization and reduction of NiIr. From the wide-angle pattern of the PXRD of the catalysts, no obvious peaks of Ni and Ir were observed (Figure 1B), which indicated the ultrafine NiIr NPs were immobilized in the pores of MOFs (vide infra).[59,60] The high stability of porous structure was further confirmed by N_2 adsorption/desorption isotherms (Figure 2). A significant

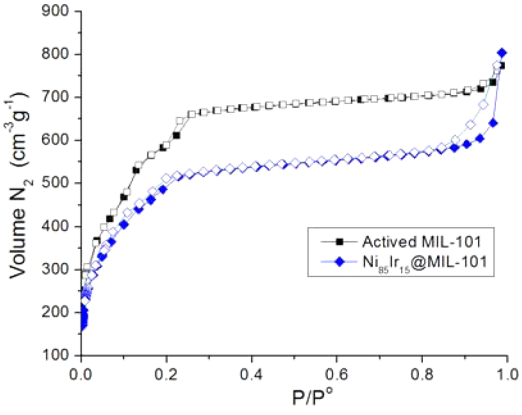

Figure 2. N_2 adsorption/desorption isotherms of activated MIL-101 and $Ni_{85}Ir_{15}$@MIL-101.

decrease of the specific areas, pore size, and pore volume between the NiIr@MIL-101 catalysts and the activated MIL-101 (Table 2, and Table S2 of the Supporting Information) strongly demonstrated that the pores of MIL-101 were filled or blocked by NiIr NPs.[61] Figure 3 shows a pattern tested by X-ray photoelectron spectroscopy (XPS) with different etch times. The signals of Ir^0 (63.7 and 60.7 eV) and Ni^0 (852.3 and 870 eV) were observed after Ar etch treatment.[36] As a result,

Table 2. BET Surface Area Results of All the Different Carrier Materials with/without Loading

carrier materials with/ without loading metals	surface area ($m^2\ g^{-1}$)	pore volume ($cm^3\ g^{-1}$)	pore diameter (nm)
MIL-101	2233	1.195	2.995
C	1030.3	1.35	6.87
SiO_2	380.0	0.89	6.79
γ-Al_2O_3	118.5	0.19	4.46
NiIr@MIL-101	1833	0.693	1.23
NiIr@C	438.2	0.91	3.65
NiIr@SiO_2	251.1	0.67	10.52
NiIr@γ-Al_2O_3	103.5	0.16	3.66

the binding energies of Ir^{4f} in the NiIr@MIL-101 nanocatalysts moved to a higher level and the binding energies of Ni^{2p} shifted to a lower level, which indicated the formation of an alloy structure. Because the preparation of XPS samples was under the air atmosphere, the peaks of oxidized Ni (856, 873.2 eV) and Ir (65.7, 62.8 eV) before etch treatment were observed. The size and shape of NiIr NPs were further characterized by transmission electron microscopy (TEM) as well as EDX analysis, as shown in Figure 4. Both signals of Ni and Ir were observed in the EDX spectra. Uniform NiIr NPs with an average size of 1.9 ± 0.4 nm were observed, indicating the NiIr NPs could be confined in the pores of MIL-101.

The catalytic activity toward the decomposition of hydrazine monohydrate was investigated in alkaline solution (0.5 M) at 50 °C (Figure 5). Large differences of the activities between the catalysts with various NiIr composition were observed. Surprisingly, the Ni@MIL-101 showed almost no activity toward the hydrogen generation of hydrazine monohydrate, and Ir@MIL-101 showed the highest TOF value (788 h^{-1}) but poor selectivity (only 6%). Considered with the activity and H_2 selectivity, $Ni_{85}Ir_{15}$@MIL-101 stands out from all the other NiIr@MIL-101 catalysts tested, with 100% hydrogen selectivity and the TOF value of 464 h^{-1} at 50 °C. Compared with all the Ir-based bimetallic catalysts previously reported, $Ni_{85}Ir_{15}$@MIL-101 exhibites the highest TOF value (Table 3). Moreover, the gas released over $Ni_{85}Ir_{15}$@MIL-101 was further detected by a mass analyzer. As shown in Figure 6, no signals of NH_3 were observed, indicating 100% H_2 selectivity. Furthermore, to demonstrate the effects of porous MIL-101 in the catalysts

DOI: 10.1021/acssuschemeng.5b00009
ACS Sustainable Chem. Eng. 2015, 3, 1086−1093

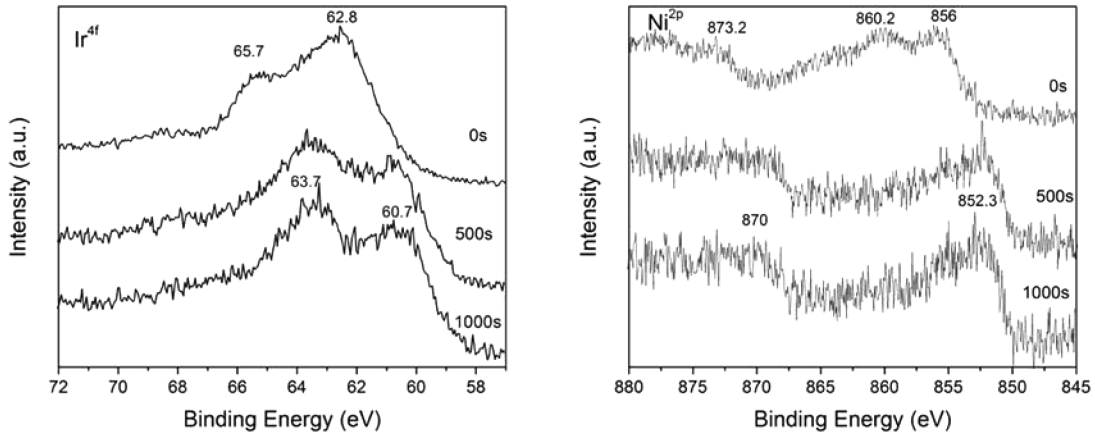

Figure 3. XPS spectra of Ir^{4f} (a) and Ni^{2p} (b) for catalyst NiIr@MIL-101 with different etch times.

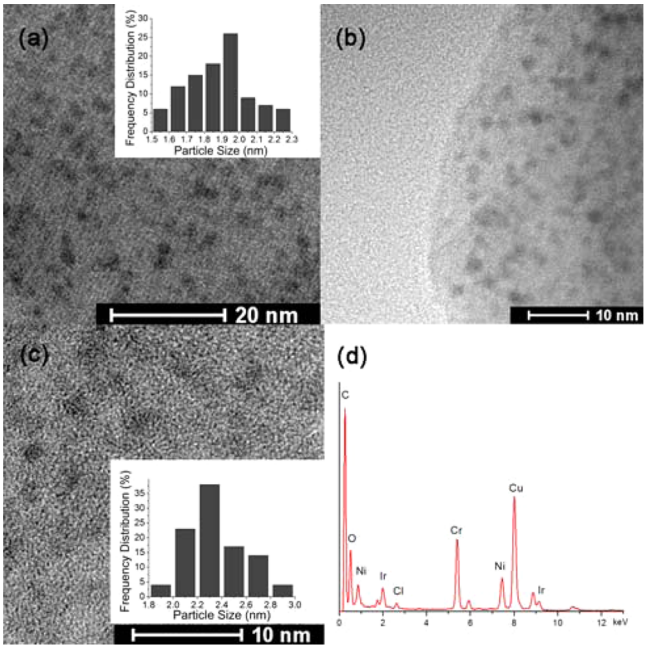

Figure 4. $Ni_{85}Ir_{15}$@MIL-101 catalyst with uniform NiIr NPs supported on porous MIL-101: (a, b) TEM of the as-synthesized catalyst, (a inset) the NiIr NPs distribution; (c) after five run uses; (d) EDX spectrum.

toward the dehydrogenation of hydrazine monohydrate, NiIr NPs supported on other carriers, including some common supports like γ-Al_2O_3, SiO_2, and carbon black were tested. In addition, the catalytic activities of the physical mixture of NiIr NPs and MIL-101 were also tested. As shown in Figure 7a, all the catalysts tested were inferior to that of NiIr@MIL-101, which highlights the dominant effect of MIL-101 toward the hydrogen generation of hydrous hydrazine. The pore size, pore volume, and surface areas of the catalysts with/without NiIr NPs loading, tested by N_2 adsorption−desorption, are listed in Table 2. For all the supports, large decreases were observed for the surface area and pore volume after the encapsulation of the metal nanoparticles. Thanks to the large pore size, window size and hybrid pore surface of MIL-101,[62] which could facilitate the immobilization of NiIr NPs with size- and shape-controlled in the confined cavities (Figure 4, and Figure S1 of the Supporting Information), and adsorption of substrate hydrazine inside the pores, and thus the NiIr@MIL-101 catalyst exhibits the highest

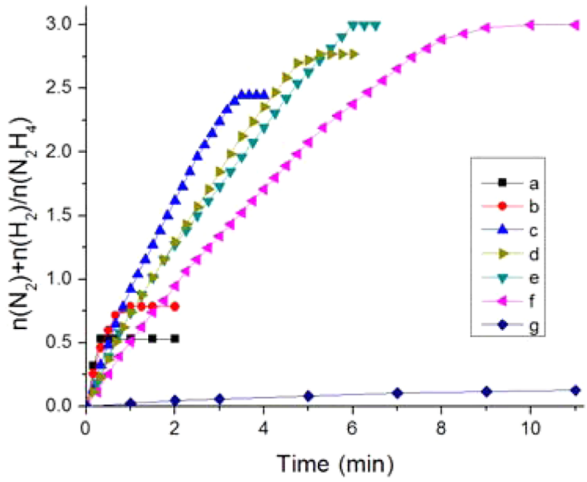

Figure 5. Time plots for the dehydrogenation of hydrazine monohydrate catalyzed by NiIr@MIL-101 catalysts in the presence of NaOH (0.5 M) at 50 °C: (a) Ir@MI-101; (b) $Ni_{49}Ir_{51}$@MIL-101; (c) $Ni_{71}Ir_{29}$@MIL-101; (d) $Ni_{82}Ir_{18}$@MIL-101; (e) $Ni_{85}Ir_{15}$@MIL-101; (f) $Ni_{90}Ir_{10}$@MIL-101; (g) Ni@MIL-101 (catalyst = 0.100 g; n_{metal}/n_{H2NNH2} = 1:10).

Table 3. Comparison of the Decompositions of Hydrazine Monohydrate Catalyzed by Catalysts in This Study and Previous Reports

catalyst	T (°C)	ratio (metal/H_2NNH_2)	TOF (h^{-1})	reference
NiFe	70	0.1	6.6	6
$Ni_{85}Ir_{15}$@MIL-101	50	0.048	464	this study
Ni_3Pt_7/graphene	50	0.5	416	30
$Ni_{66}Rh_{34}$@ZIF-8	50	0.141	140	59
$Ni_{64.1}Mo_{11.5}B_{24.4}$-$La(OH)_3$	50	0.3	13.3	24
$Ni_{0.6}Fe_{0.4}Mo$	50	0.2	28.8	38
$NiPt_{0.057}/Al_2O_3$	30	0.45	16.5	64
$Ni_{85}Ir_{15}$@MIL-101	25	0.048	24	this study
Ni_3Pt_7/graphene	25	0.5	68	30
Rh_4Ni	25	0.1	9.6	23
$Ni_{0.95}Ir_{0.05}$-CTAB	25	0.1	1.6	36
$Ni_{60}Pt_{40}$	25	0.1	150	35
PdIr	25	0.25	2.6	46

DOI: 10.1021/acssuschemeng.5b00009
ACS Sustainable Chem. Eng. 2015, 3, 1086−1093

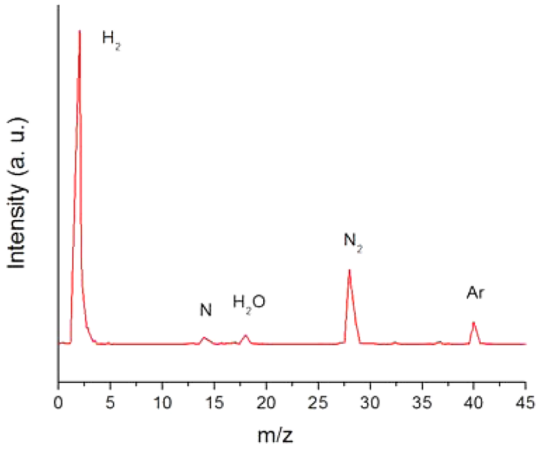

Figure 6. MS spectrum of the mixture of gases collected from the hydrogen generation of $N_2H_4{\cdot}H_2O$ catalyzed by $Ni_{85}Ir_{15}$@MIL-101 catalyst (catalyst = 0.100 g; n_{metal}/n_{H2NNH2} = 1:10) at 50 °C.

catalytic activity toward hydrogen generation from alkaline solution of hydrazine. Furthermore, only 2.35 equiv gas and 78.3% hydrogen selectivity were obtained after 1.5 h for the physical mixture of NiIr NPs and MIL-101, indicating the key factor of MOFs in promoting decomposition of hydrazine monohydrate. It is the host−guest cooperation between nanoparticles and MOF that greatly improves H_2 selectivity. The limited window size of MIL-101 prevents NiIr NPs from crossing the cavities, thus minimizing the possibility of aggregation of NiIr NPs.[60,63] The physical mixture of Ni@MIL-101 and Ir@MIL-101 exhibited little catalytic performance and almost no activity was observed for MIL-101, indicating the synergistic effect of Ni and Ir in the molecular-scale level is the key for enhancement of their catalytic activity (Figure 7b). The catalyst surface was modified by strong intermetallic electronic interactions between Ni and Ir, which may significantly tune the bonding pattern of the catalyst surface and stabilize the reaction intermediates, resulting in enhanced the catalytic activity and selectivity (Scheme S1 of the Supporting Information).[6,23,31] The decomposition of $N_2H_4{\cdot}H_2O$ contains two types of bond-dissociation including N−N and N−H breakage. The intermediate product of $\cdot NH_2$ radical is formed through N−N bond dissociation. However, further N−H bond cracking to form hydrogen molecules is more difficult than to form NH_3 by the combination of $\cdot NH_2$ and H· due to the external energy needed. In this system, the dissociation of N−H can be selected by NiIr@MIL-101 for hydrogen generation. To test the effect of alkaline toward the decomposition of the hydrazine monohydrate, the catalytic performance was checked without adding NaOH (Figure 8). As a result, the reactivity and H_2 selectivity in the alkaline system were much higher than that in the absence of adding NaOH, which may be caused by the acceleration of rate-determining step of hydrazine decomposition ($N_2H_4 \rightarrow N_2H_3^* + H^*$) and suppresses the formation of basic NH_3 by NaOH.[61]

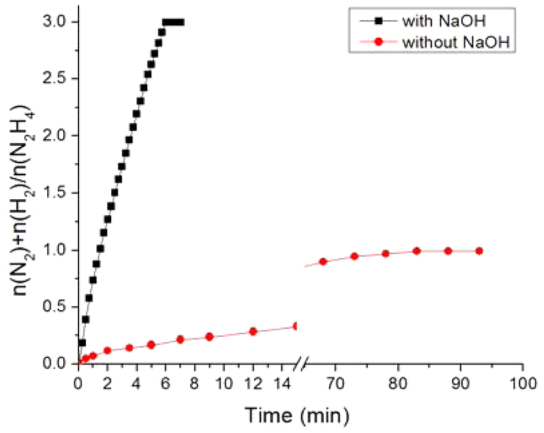

Figure 8. Time plots for the hydrogen generation of $N_2H_4{\cdot}H_2O$ catalyzed by $Ni_{85}Ir_{15}$@MIL-101 catalyst with/without alkaline (0.5 M NaOH) at 50 °C. (catalyst = 0.100 g; n_{metal}/n_{H2NNH2} = 1:10).

To obtain the Arrhenius activation energy, the dehydrogenation reactions were performed at 25, 40, 50, and 60 °C, respectively (Figure 9a). The E_a was calculated as 66.9 kJ mol^{-1} (Figure 9b), which is a close to the previous report.[24,28,59] To our delight, even at 25 °C, the $Ni_{85}Ir_{15}$@MIL-101 exhibits 100% hydrogen selectivity with a TOF value of 24 h^{-1}.

The reusability of $Ni_{85}Ir_{15}$@MIL-101 was tested by successively adding the same amount of hydrazine monohydrate after the accomplishment of the previous hydrogen generation at 50 °C. Figure 10 shows a result of little decreasing of catalytic performance after five runs, but the H_2 selectivity

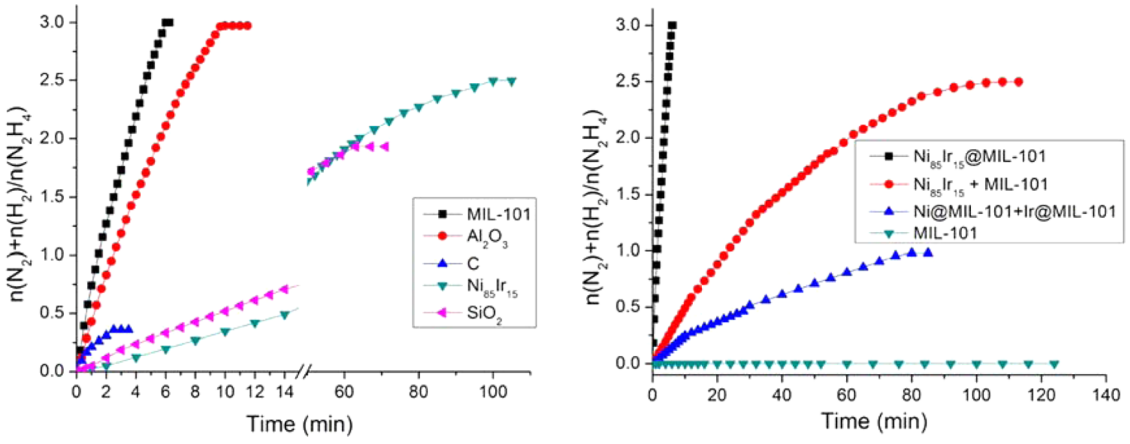

Figure 7. Time plots of the hydrogen generation of $N_2H_4{\cdot}H_2O$ catalyzed by different catalysts in alkaline solution (0.5 M NaOH) at 50 °C: (a) by $Ni_{85}Ir_{15}$ NPs with different supported materials; (b) by $Ni_{85}Ir_{15}$ NPs without support, activated MIL-101, physical mixture of $Ni_{85}Ir_{15}$ NPs and MIL-101, physical mixture of Ir@MIL-101 and Ni@MIL-101. (catalyst = 0.100 g; n_{metal}/n_{H2NNH2} = 1:10).

DOI: 10.1021/acssuschemeng.5b00009
ACS Sustainable Chem. Eng. 2015, 3, 1086−1093

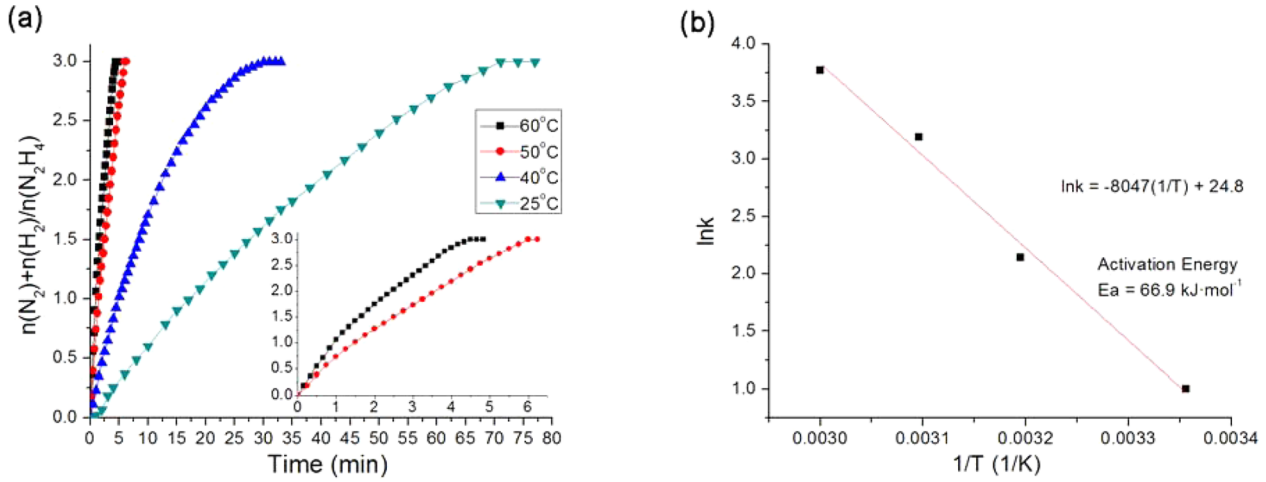

Figure 9. (a) Time plots for the decomposition of $N_2H_4{\cdot}H_2O$ catalyzed by $Ni_{85}Ir_{15}$@MIL-101 catalyst at different temperatures (catalyst = 0.100 g; n_{metal}/n_{H2NNH2} = 1:10), (inset) magnification of the initial 6 min. (b) linear fitting of ln k vs $1/T$ (k = the gas generation rate in the line part at different temperatures).

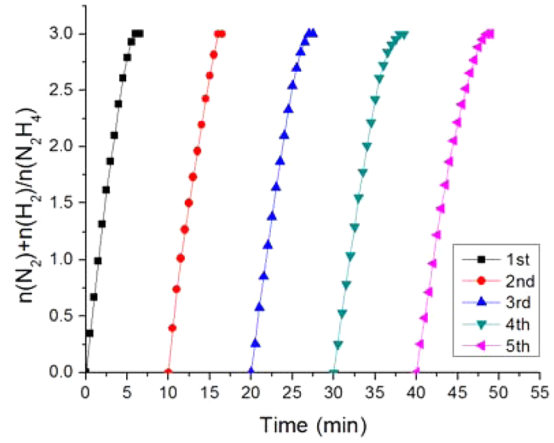

Figure 10. Five runs of the decomposition of $N_2H_4{\cdot}H_2O$ catalyzed by $Ni_{85}Ir_{15}$@MIL-101 catalyst in alkaline solution (0.5 M NaOH) at 50 °C (catalyst = 0.100 g; n_{metal}/n_{H2NNH2} = 1:10).

remained 100%. From the PXRD in Figure 1, there is no change of the as-synthesized catalyst after a five run test. Furthermore, Figure 4c indicates that the NPs remain well-dispersed after a five run test; however, the average diameter was increased to 2.5 ± 0.4 nm, which may be the major factor for the slight decrease of the catalytic activity. Further work for the improvement of the catalysts including the stability and performance is still underway.

CONCLUSION

In summary, bimetallic NiIr NPs were successfully encapsulated on the pores of MIL-101 by a simple liquid impregnation method. Thanks to the unique porous structure of MIL-101 and the synergetic effect, the catalytic activity of NiIr NPs has been enhanced, to a great extent, with 100% H_2 selectivity and good durability toward dehydrogenation of hydrazine monohydrate after being immobilized into the pores of MIL-101. The combination of high catalytic activity and selectivity makes $Ni_{85}Ir_{15}$@MIL-101 a potential catalyst for dehydrogenation of alkaline solution of hydrazine for chemical hydrogen storage.

ASSOCIATED CONTENT

Supporting Information

More detailed information about the BET and TEM of the NiIr@MIL-101 catalysts. The Supporting Information is available free of charge on the ACS Publications website at DOI: 10.1021/acssuschemeng.5b00009.

AUTHOR INFORMATION

Corresponding Authors

*W. Luo. E-mail: wluo@whu.edu.cn. Tel.: +86 2768752366.
*G. Cheng. E-mail: gzcheng@whu.edu.cn.

Notes

The authors declare no competing financial interest.

ACKNOWLEDGMENTS

This work was financially supported by the National Natural Science Foundation of China (21201134), the Natural Science Foundation of Jiangsu Province (BK20130370), the Natural Science Foundation of Hubei Province (2013CFB288), the Creative Research Groups of Hubei Province (2014CFA007) and Large-scale Instrument and Equipment Sharing Foundation of Wuhan University.

REFERENCES

(1) Dunn, S. Hydrogen futures: Toward a sustainable energy system. *Int. J. Hydrogen Energy* **2002**, *27* (3), 235−264.
(2) Schultz, M. G.; Diehl, T.; Brasseur, G. P.; Zittel, W. Air pollution and climate-forcing impacts of a global hydrogen economy. *Science* **2003**, *302* (5645), 624−627.
(3) Wu, G.; Zhang, C.; Li, S.; Han, Z.; Wang, T.; Ma, X.; Gong, J. Hydrogen production via glycerol steam reforming over Ni/Al_2O_3: Influence of nickel precursors. *ACS Sustainable Chem. Eng.* **2013**, *1* (8), 1052−1062.
(4) Schlapbach, L.; Züttel, A. Hydrogen-storage materials for mobile applications. *Nature* **2001**, *414* (6861), 353−358.
(5) Loges, B.; Boddien, A.; Junge, H.; Beller, M. Controlled generation of hydrogen from formic acid amine adducts at room temperature and application in H_2/O_2 fuel cells. *Angew. Chem., Int. Ed.* **2008**, *47* (21), 3962−3965.
(6) Singh, S. K.; Singh, A. K.; Aranishi, K.; Xu, Q. Noble-metal-free bimetallic nanoparticle-catalyzed selective hydrogen generation from hydrous hydrazine for chemical hydrogen storage. *J. Am. Chem. Soc.* **2011**, *133* (49), 19638−19641.

DOI: 10.1021/acssuschemeng.5b00009
ACS Sustainable Chem. Eng. 2015, 3, 1086−1093

(7) Schüth, F.; Bogdanović, B.; Felderhoff, M. Light metal hydrides and complex hydrides for hydrogen storage. *Chem. Commun.* **2004**, *20*, 2249−2258.
(8) Chen, J.; Lang, Z.; Xu, Q.; Hu, B.; Fu, J.; Chen, Z.; Zhang, J. Facile preparation of monodisperse carbon spheres: Template-free construction and their hydrogen storage properties. *ACS Sustainable Chem. Eng.* **2013**, *1* (8), 1063−1068.
(9) Gong, J.; Michalkiewicz, B.; Chen, X.; Mijowska, E.; Liu, J.; Jiang, Z.; Wen, X.; Tang, T. Sustainable conversion of mixed plastics into porous carbon nanosheets with high performances in uptake of carbon dioxide and storage of hydrogen. *ACS Sustainable Chem. Eng.* **2014**, *2* (12), 2837−2844.
(10) Guo, C. X.; Wang, Y.; Li, C. M. Hierarchical graphene-based material for over 4.0 wt% physisorption hydrogen storage capacity. *ACS Sustainable Chem. Eng.* **2012**, *1* (1), 14−18.
(11) Luo, W.; Campbell, P. G.; Zakharov, L. N.; Liu, S.-Y. A single-component liquid-phase hydrogen storage material. *J. Am. Chem. Soc.* **2011**, *133* (48), 19326−19329.
(12) Yang, L.; Luo, W.; Cheng, G. Graphene-supported Ag-based core−shell nanoparticles for hydrogen generation in hydrolysis of ammonia borane and methylamine borane. *ACS Appl. Mater. Interfaces* **2013**, *5* (16), 8231−8240.
(13) Hsu, S. F.; Rommel, S.; Eversfield, P.; Muller, K.; Klemm, E.; Thiel, W. R.; Plietker, B. A rechargeable hydrogen battery based on Ru catalysis. *Angew. Chem., Int. Ed.* **2014**, *53* (27), 7074−7078.
(14) Wang, Z. L.; Yan, J. M.; Ping, Y.; Wang, H. L.; Zheng, W. T.; Jiang, Q. An efficient CoAuPd/C catalyst for hydrogen generation from formic acid at room temperature. *Angew. Chem., Int. Ed.* **2013**, *52* (16), 4406−4409.
(15) Dai, H.; Cao, N.; Yang, L.; Su, J.; Cheng, G. AgPd nanoparticles supported on MIL-101 as high performance catalysts for catalytic dehydrogenation of formic acid. *J. Mater. Chem. A* **2014**, *2* (29), 11060−11064.
(16) Jia, L.; Bulushev, D. A.; Beloshapkin, S.; Ross, J. R. Hydrogen production from formic acid vapour over a Pd/C catalyst promoted by potassium salts: Evidence for participation of buffer-like solution in the pores of the catalyst. *Appl. Catal., B* **2014**, *160*, 35−43.
(17) Czaun, M.; Goeppert, A.; Kothandaraman, J.; May, R. B.; Haiges, R.; Prakash, G. S.; Olah, G. A. Formic acid as a hydrogen storage medium: Ruthenium-catalyzed generation of hydrogen from formic acid in emulsions. *ACS Catal.* **2013**, *4* (1), 311−320.
(18) Jiang, K.; Xu, K.; Zou, S.; Cai, W.-B. B-Doped Pd catalyst: Boosting room-temperature hydrogen production from formic acid−formate solutions. *J. Am. Chem. Soc.* **2014**, *136* (13), 4861−4864.
(19) Amende, M.; Gleichweit, C.; Werner, K.; Schernich, S.; Zhao, W.; Lorenz, M. P.; Höfert, O.; Papp, C.; Koch, M.; Wasserscheid, P. Model catalytic studies of liquid organic hydrogen carriers: Dehydrogenation and decomposition mechanisms of dodecahydro-N-ethylcarbazole on Pt(111). *ACS Catal.* **2014**, *4* (2), 657−665.
(20) Amende, M.; Gleichweit, C.; Schernich, S.; Höfert, O.; Lorenz, M. P.; Zhao, W.; Koch, M.; Obesser, K.; Papp, C.; Wasserscheid, P. Size and structure effects controlling the stability of the liquid organic hydrogen carrier dodecahydro-N-ethylcarbazole during dehydrogenation over Pt model catalysts. *J. Phys. Chem. Lett.* **2014**, *5* (8), 1498−1504.
(21) Brückner, N.; Obesser, K.; Bösmann, A.; Teichmann, D.; Arlt, W.; Dungs, J.; Wasserscheid, P. Evaluation of industrially applied heat-transfer fluids as liquid organic hydrogen carrier systems. *ChemSusChem* **2014**, *7* (1), 229−235.
(22) Yang, M.; Dong, Y.; Fei, S.; Pan, Q.; Ni, G.; Han, C.; Ke, H.; Fang, Q.; Cheng, H. Hydrogenation of N-propylcarbazole over supported ruthenium as a new prototype of liquid organic hydrogen carriers (LOHC). *RSC Adv.* **2013**, *3* (47), 24877−24881.
(23) Singh, S. K.; Xu, Q. Complete conversion of hydrous hydrazine to hydrogen at room temperature for chemical hydrogen storage. *J. Am. Chem. Soc.* **2009**, *131* (50), 18032−18033.
(24) Zhang, J.; Kang, Q.; Yang, Z.; Dai, H.; Zhuang, D.; Wang, P. A cost-effective NiMoB−La$(OH)_3$ catalyst for hydrogen generation from decomposition of alkaline hydrous hydrazine solution. *J. Mater. Chem. A* **2013**, *1* (38), 11623−11628.
(25) Cao, N.; Su, J.; Luo, W.; Cheng, G. Hydrolytic dehydrogenation of ammonia borane and methylamine borane catalyzed by graphene supported Ru@ Ni core−shell nanoparticles. *Int. J. Hydrogen Energy* **2014**, *39* (1), 426−435.
(26) Xia, B.; Cao, N.; Dai, H.; Su, J.; Wu, X.; Luo, W.; Cheng, G. Bimetallic nickel−rhodium nanoparticles supported on ZIF-8 as highly efficient catalysts for hydrogen generation from hydrazine in alkaline solution. *ChemCatChem* **2014**, *6* (9), 2549−2552.
(27) Du, Y.; Su, J.; Luo, W.; Cheng, G. Graphene-supported nickel-platinum nanoparticles as efficient catalyst for hydrogen generation from hydrous hydrazine at room temperature. *ACS Appl. Mater. Interfaces* **2015**, *7* (2), 1031−1034.
(28) Cao, N.; Su, J.; Luo, W.; Cheng, G. Ni−Pt nanoparticles supported on MIL-101 as highly efficient catalysts for hydrogen generation from aqueous alkaline solution of hydrazine for chemical hydrogen storage. *Int. J. Hydrogen Energy* **2014**, *39* (18), 9726−9734.
(29) Cao, N.; Yang, L.; Dai, H.; Liu, T.; Su, J.; Wu, X.; Luo, W.; Cheng, G. Immobilization of ultrafine bimetallic Ni−Pt nanoparticles inside the pores of metal−organic frameworks as efficient catalysts for dehydrogenation of alkaline solution of hydrazine. *Inorg. Chem.* **2014**, *53* (19), 10122−10128.
(30) Cao, N.; Yang, L.; Du, C.; Su, J.; Luo, W.; Cheng, G. Highly efficient dehydrogenation of hydrazine over graphene supported flower-like Ni−Pt nanoclusters at room temperature. *J. Mater. Chem. A* **2014**, *2* (35), 14344−14347.
(31) Singh, S. K.; Iizuka, Y.; Xu, Q. Nickel-palladium nanoparticle catalyzed hydrogen generation from hydrous hydrazine for chemical hydrogen storage. *Int. J. Hydrogen Energy* **2011**, *36* (18), 11794−11801.
(32) Hazari, N. Homogeneous iron complexes for the conversion of dinitrogen into ammonia and hydrazine. *Chem. Soc. Rev.* **2010**, *39* (11), 4044−4056.
(33) Takahashi, T.; Mizobe, Y.; Sato, M.; Uchida, Y.; Hidai, M. Preparation and properties of molybdenum-and tungsten-dinitrogen complexes. 10. Conversion of ligating dinitrogen into hydrazine with hydrazido (1-) complexes as intermediates. *J. Am. Chem. Soc.* **1979**, *101* (12), 3405−3407.
(34) Bossard, G.; George, T. A.; Howell, D. B.; Koczon, L. M.; Lester, R. K. Reactions of coordinated dinitrogen. 12. Identification of intermediates in the conversion of molybdenum-bound dinitrogen into ammonia and hydrazine. Factors affecting the ammonia-forming reaction. *Inorg. Chem.* **1983**, *22* (14), 1968−1970.
(35) Singh, A. K.; Xu, Q. Highly-dispersed surfactant-free bimetallic Ni−Pt nanoparticles as high-performance catalyst for hydrogen generation from hydrous hydrazine. *Int. J. Hydrogen Energy* **2014**, *39* (17), 9128−9134.
(36) Singh, S. K.; Xu, Q. Bimetallic nickel-iridium nanocatalysts for hydrogen generation by decomposition of hydrous hydrazine. *Chem. Commun.* **2010**, *46* (35), 6545−6547.
(37) Sun, J.-K.; Xu, Q. Metal nanoparticles immobilized on carbon nanodots as highly active catalysts for hydrogen generation from hydrazine in aqueous solution. *ChemCatChem* **2015**, *7* (3), 526−531.
(38) Wang, H.-L.; Yan, J.-M.; Li, S.-J.; Zhang, X.-W.; Jiang, Q. Noble-metal-free NiFeMo nanocatalyst for hydrogen generation from the decomposition of hydrous hydrazine. *J. Mater. Chem. A* **2014**, *3* (1), 121−124.
(39) Wang, J.; Li, Y.; Zhang, Y. Precious-metal-free nanocatalysts for highly efficient hydrogen production from hydrous hydrazine. *Adv. Funct. Mater.* **2014**, *24* (45), 7073−7077.
(40) He, L.; Huang, Y.; Wang, A.; Wang, X.; Chen, X.; Delgado, J. J.; Zhang, T. A noble-metal-free catalyst derived from Ni-Al hydrotalcite for hydrogen generation from $N_2H_4{\cdot}H_2O$ decomposition. *Angew. Chem.* **2012**, *124* (25), 6295−6298.
(41) Zhu, Q.-L.; Zhong, D.-C.; Demirci, U. B.; Xu, Q. Controlled synthesis of ultrafine surfactant-free NiPt nanocatalysts towards efficient and complete hydrogen generation from hydrazine borane at room temperature. *ACS Catal.* **2014**, *4* (12), 4261−4268.

DOI: 10.1021/acssuschemeng.5b00009
ACS Sustainable Chem. Eng. 2015, 3, 1086−1093

(42) Jang, I. J.; Shin, H. S.; Shin, N. R.; Kim, S. H.; Kim, S. K.; Yu, M. J.; Cho, S. J. Macroporous−mesoporous alumina supported iridium catalyst for hydrazine decomposition. *Catal. Today* **2012**, *185* (1), 198−204.
(43) Cho, S. J.; Lee, J.; Lee, Y. S.; Kim, D. P. Characterization of iridium catalyst for decomposition of hydrazine hydrate for hydrogen generation. *Catal. Lett.* **2006**, *109* (3−4), 181−186.
(44) Vieira, R.; Bernhardt, P.; Ledoux, M.-J.; Pham-Huu, C. Performance comparison of Ir/CNF and Ir/Al_2O_3 catalysts in a 2 N hydrazine microthruster. *Catal. Lett.* **2005**, *99* (3−4), 177−180.
(45) He, L.; Huang, Y.; Liu, X. Y.; Li, L.; Wang, A.; Wang, X.; Mou, C.-Y.; Zhang, T. Structural and catalytic properties of supported Ni-Ir alloy catalysts for H_2 generation via hydrous hydrazine decomposition. *Appl. Catal., B* **2014**, *147*, 779−788.
(46) Liu, M.; Zheng, Y.; Xie, S.; Li, N.; Lu, N.; Wang, J.; Kim, M. J.; Guo, L.; Xia, Y. Facile synthesis of Pd−Ir bimetallic octapods and nanocages through galvanic replacement and co-reduction, and their use for hydrazine decomposition. *Phys. Chem. Chem. Phys.* **2013**, *15* (28), 11822−11829.
(47) Aijaz, A.; Xu, Q. Catalysis with metal nanoparticles immobilized within the pores of metal-organic frameworks. *J. Phys. Chem. Lett.* **2014**, *5* (8), 1400−1411.
(48) Garcia-Garcia, P.; Muller, M.; Corma, A. MOF catalysis in relation to their homogeneous counterparts and conventional solid catalysts. *Chem. Sci.* **2014**, *5* (8), 2979−3007.
(49) Zhu, Q.-L.; Xu, Q. Metal−organic framework composites. *Chem. Soc. Rev.* **2014**, *43* (16), 5468−5512.
(50) Balbuena, P. B.; Yu, J. How impurities affect CO_2 capture in metal-organic frameworks modified with different functional groups. *ACS Sustainable Chem. Eng.* **2014**, *3*, 117−124.
(51) Na, K.; Choi, K. M.; Yaghi, O. M.; Somorjai, G. A. Metal nanocrystals embedded in single nanocrystals of MOFs give unusual selectivity as heterogeneous catalysts. *Nano Lett.* **2014**, *14* (10), 5979−5983.
(52) Zhao, Y.; Zhang, J.; Song, J.; Li, J.; Liu, J.; Wu, T.; Zhang, P.; Han, B. Ru nanoparticles immobilized on metal−organic framework nanorods by supercritical CO_2-methanol solution: Highly efficient catalyst. *Green Chem.* **2011**, *13* (8), 2078−2082.
(53) Czaja, A. U.; Trukhan, N.; Müller, U. Industrial applications of metal−organic frameworks. *Chem. Soc. Rev.* **2009**, *38* (5), 1284−1293.
(54) Zahmakiran, M. Iridium nanoparticles stabilized by metal organic frameworks (IrNPs@ ZIF-8): Synthesis, structural properties and catalytic performance. *Dalton. Trans.* **2012**, *41* (41), 12690−12696.
(55) Pan, Y.; Yuan, B.; Li, Y.; He, D. Multifunctional catalysis by Pd@ MIL-101: One-step synthesis of methyl isobutyl ketone over palladium nanoparticles deposited on a metal−organic framework. *Chem. Commun.* **2010**, *46* (13), 2280−2282.
(56) Sarawade, P.; Tan, H.; Polshettiwar, V. Shape-and morphology-controlled sustainable synthesis of Cu, Co, and in metal organic frameworks with high CO_2 capture capacity. *ACS Sustainable Chem. Eng.* **2012**, *1* (1), 66−74.
(57) Maruyama, J.; Hasegawa, T.; Iwasaki, S.; Kanda, H.; Kishimoto, H. Heat treatment of carbonized hemoglobin with ammonia for enhancement of pore development and oxygen reduction activity. *ACS Sustainable Chem. Eng.* **2013**, *2* (3), 493−499.
(58) Férey, G.; Mellot-Draznieks, C.; Serre, C.; Millange, F.; Dutour, J.; Surblé, S.; Margiolaki, I. A chromium terephthalate-based solid with unusually large pore volumes and surface area. *Science* **2005**, *309* (5743), 2040−2042.
(59) Xia, B.; Cao, N.; Dai, H.; Su, J.; Wu, X.; Luo, W.; Cheng, G. Bimetallic nickel-rhodium nanoparticles supported on ZIF-8 as highly efficient catalysts for hydrogen generation from hydrazine in alkaline solution. *ChemCatChem* **2014**, *6* (9), 2549−2552.
(60) Aijaz, A.; Karkamkar, A.; Choi, Y. J.; Tsumori, N.; Rönnebro, E.; Autrey, T.; Shioyama, H.; Xu, Q. Immobilizing highly catalytically active Pt nanoparticles inside the pores of metal−organic framework: A double solvents approach. *J. Am. Chem. Soc.* **2012**, *134* (34), 13926−13929.
(61) Gu, X.; Lu, Z.-H.; Jiang, H.-L.; Akita, T.; Xu, Q. Synergistic catalysis of metal−organic framework-immobilized Au−Pd nanoparticles in dehydrogenation of formic acid for chemical hydrogen storage. *J. Am. Chem. Soc.* **2011**, *133* (31), 11822−11825.
(62) Li, J.; Zhu, Q.-L.; Xu, Q. Non-noble bimetallic CuCo nanoparticles encapsulated in the pores of metal−organic frameworks: Synergetic catalysis in the hydrolysis of ammonia borane for hydrogen generation. *Catal. Sci. Technol.* **2015**, *5* (1), 525−530.
(63) Zhu, Q.-L.; Li, J.; Xu, Q. Immobilizing metal nanoparticles to metal−organic frameworks with size and location control for optimizing catalytic performance. *J. Am. Chem. Soc.* **2013**, *135* (28), 10210−10213.
(64) He, L.; Huang, Y.; Wang, A.; Liu, Y.; Liu, X.; Chen, X.; Delgado, J. J.; Wang, X.; Zhang, T. Surface modification of Ni/Al_2O_3 with Pt: Highly efficient catalysts for H_2 generation via selective decomposition of hydrous hydrazine. *J. Catal.* **2013**, *298*, 1−9.

DOI: 10.1021/acssuschemeng.5b00009
ACS Sustainable Chem. Eng. 2015, 3, 1086−1093